Analysis of the present and future winter Pacific-North American teleconnection in the ECHAM5 global and RegCM3 regional climate models

Clim Dyn (2014) 42:1671–1682
DOI 10.1007/s00382-013-1910-x

Analysis of the present and future winter Pacific-North American teleconnection in the ECHAM5 global and RegCM3 regional climate models

Andrea M. Allan · Steven W. Hostetler · Jay R. Alder

Received: 16 November 2012 / Accepted: 6 August 2013 / Published online: 18 August 2013

Abstract We use the NCEP/NCAR Reanalysis (NCEP) and the MPI/ECHAM5 general circulation model to drive the RegCM3 regional climate model to assess the ability of the models to reproduce the spatiotemporal aspects of the Pacific-North American teleconnection (PNA) pattern. Composite anomalies of the NCEP-driven RegCM3 simulations for 1982–2000 indicate that the regional model is capable of accurately simulating the key features (500-hPa heights, surface temperature, and precipitation) of the positive and negative phases of the PNA with little loss of information in the downscaling process. The basic structure of the PNA is captured in both the ECHAM5 global and ECHAM5-driven RegCM3 simulations. The 1950–2000 ECHAM5 simulation displays similar temporal and spatial variability in the PNA index as that of NCEP; however, the magnitudes of the positive and negative phases are weaker than those of NCEP. The RegCM3 simulations clearly differentiate the climatology and associated anomalies of snow water equivalent and soil moisture of the positive and negative PNA phases. In the RegCM3 simulations of the future (2050–2100), changes in the location and extent of the Aleutian low and the continental high over North America alter the dominant flow patterns associated with positive and negative PNA modes. The future projections display a shift in the patterns of the relationship between the PNA and surface climate variables, which suggest the potential for changes in the PNA-related surface hydrology of North America.

Keywords Climate change · Regional downscaling · PNA teleconnection · Coupled climate models · North American climate

A. M. Allan (✉)
104 CEOAS Admin Bldg, College of Earth, Ocean, and Atmospheric Sciences, Oregon State University, Corvallis, OR 97331, USA
e-mail: aallan@coas.oregonstate.edu

S. W. Hostetler · J. R. Alder
U.S. Geological Survey, 104 CEOAS Admin Bldg, College of Earth, Ocean, and Atmospheric Sciences, Oregon State University, Corvallis, OR 97331, USA

1 Introduction

The Pacific-North American teleconnection (PNA) pattern is defined by a quasi-stationary wave field that has long been recognized as a prominent feature of Northern Hemisphere (NH) atmospheric circulation (Wallace and Gutzler 1981; Barnston and Livezey 1987). The PNA varies from intra-seasonal (2–90 days) to inter-annual (2–20 years) time scales (Feldstein 2000) and is a primary control of winter climate variability in the North Pacific and North America (Müller and Roeckner 2006; Notaro et al. 2006). Although the PNA is present throughout the year, the influence of the PNA on climate typically diminishes through the spring and summer, and is re-established in late autumn (Leathers et al. 1991). In extreme cases, the PNA can be shown to influence the loss of sea ice in the NH, which is a result of strong anticyclonic flow over the western Arctic (L'Heureux et al. 2008). The PNA is characterized by the PNA index (PNAI), which is computed as the average of standardized 500-hPa geopotential heights at four locations over the Pacific Ocean and North America, and typically ranges in value from −3 to +3. As such, the PNAI is a quantitative measure of the meridional (the positive phase, PNA+) or zonal (the negative phase, PNA−) 500-hPa geostrophic wind flow relative to the climatological mean. Variations in 500-hPa

geopotential heights drive changes in atmospheric circulation associated with the NH polar jet stream which, in turn, affect surface climate. Over the Pacific Northwest, for example, PNA+phases from December through February (DJF) are significantly correlated with positive temperature and precipitation anomalies, whereas DJF PNA− phases are associated with negative temperature and precipitation anomalies (Wallace and Gutzler 1981; Leathers et al. 1991).

The relationships between the PNA, temperature, and precipitation establish antecedent conditions for slightly less well-defined correlations between the PNA and season-ahead hydrologic conditions, such as March snow water equivalent and April soil moisture (Coleman and Rogers 2003; Ge et al. 2009). Since the 1950s, there has been a shift of the PNA toward more frequent positive modes during the late winter months (Leathers and Palecki 1992; Lee et al. 2011; Pederson et al. 2013). Combined with NH warming, the warm winters associated with these more frequent positive modes has led to decreases in the amount and extent of mountain snowpack and earlier onset of spring snow melt (Abatzoglou 2010; McCabe and Wolock 2010). In the Ohio River Valley, the sign of the PNAI is associated with regional hydrologic conditions: extreme negative PNA– winters can result in as much as a 100 % increase in stream flow relative to the mean winter for the twentieth century (Coleman and Rogers 2003). Positive PNA phases have also been linked to wildfire activity, particularly in the Southern Canadian Rockies where warmer winter temperatures and reduced precipitation can lead to drier conditions during the following summer fire season (Fauria and Johnson 2008).

Numerous studies have analyzed the PNA in observations and climate model simulations; however, few of these explore how the simulated PNA influences North American climate, particularly in the future, and those that have are somewhat limited temporally and spatially (e.g. Lau 1981; Notaro et al. 2006). Kawamura et al. (1995) applied a low-resolution GCM to simulate low-frequency modes of climate variability in the northern extratropics. A rotated empirical orthogonal function (rEOF) analysis revealed the PNA as the leading winter mode in observations and the third leading mode in the simulation. When compared to observations, the modeled PNA exhibited a very similar spatial pattern; however, spatial variability at interannual and interdecadal time scales differed from observations. Yu and Zwiers (2007) examined the interaction of the PNA with the El Niño-Southern Oscillation (ENSO) and the Pacific Decadal Oscillation (PDO) in 1,000 years of output from the Canadian Centre for Climate Modelling and Analysis coupled general circulation model (GCM). They found that the GCM resolved the PNA, ENSO, and the PDO and that the expression of the teleconnections compared well with observations, but they did not specifically explore the behavior of the PNA and climate. Stoner et al. (2009) provide a more comprehensive study on the ability of the GCMs included in the Fourth Assessment Report of the Intergovernmental Panel on Climate Change (IPCC AR4) to simulate the spatiotemporal characteristics of six global teleconnections, including the PNA. They discovered all but two GCMs were able to reproduce a realistic PNA pattern; however, most models were unable to capture the exact temporal variability produced by the PNA in observations. The authors did not explore the influence of these teleconnections on climate, nor did they investigate the presence of the teleconnections in future climate model projections.

Given the influence of the PNA on North American climate and hydrology, it is worthwhile exploring with climate models how the circulation pattern and associated surface climate fields might change in the future. Here we evaluate the fidelity of propagating the PNA from the National Center for Environmental Prediction and National Center for Atmospheric Research (NCEP/NCAR) global reanalysis through the RegCM3 regional climate model (RCM). We evaluate the temporal and spatial characteristics of the PNA in the Max-Planck Institute ECHAM5 GCM (hereafter ECHAM5) and analyze the atmospheric and surface response of the PNA in multi-decadal simulations of the present and future we conducted by driving the RegCM3 with ECHAM5. The high-resolution RegCM3 simulations make it possible to analyze the effects of topography on surface climate that are not resolved on the coarser GCM grids, particularly hydrologic responses in higher elevations. Furthermore, we are not aware of any studies that have examined the propagation of a large-scale teleconnection pattern, such as the PNA, from a GCM to an RCM.

In the next section we describe the models, data, and methods we used to calculate the spatial patterns of PNA and the PNAI. In Sect. 3 we evaluate the GCM-RCM coupling and assess the changes in temporal and spatial variability between the present and future climate simulations, and in Sect. 4 we conclude with a discussion of the results.

2 Methods

2.1 Models and data

We employ the NCEP/NCAR Reanalysis data (Kalnay et al. 1996) both as the basis for comparison and to drive the RegCM3. The reanalysis is produced by assimilating a large array of surface and atmospheric data into the NCEP global forecast model, which is run at T62 horizontal resolution (~2 latitude × 2 longitude) with 23 atmospheric

layers. We also use output from ECHAM5, the coupled global atmosphere–ocean GCM developed by the Max-Planck Institute for Meteorology (Roeckner et al. 2003; Jungclaus et al. 2005; Marsland et al. 2003), to drive the RegCM3. The atmospheric component of ECHAM5 has T63 horizontal resolution ($\sim$1.875° latitude × 1.875° longitude) and 31 atmospheric levels, and the ocean component has a 1.5° latitude × 1.5° longitude grid and 40 depth levels.

The RegCM3 (Pal et al. 2000, 2007) was originally developed at NCAR and is now supported by the Abdus Salam International Centre for Theoretical Physics. For this study, our configuration of the RegCM3 includes a 50-km horizontal grid that spans $\sim$12°–75°N latitude and $\sim$20°–175°W longitude, 23 atmospheric layers, the Grell convective precipitation scheme (Grell 1993), and the Biosphere–Atmosphere Transfer Scheme (Dickinson et al. 1993) that simulates the exchange of radiation, momentum, heat, and moisture between the boundary layer and the surface. The boundary conditions (vertical profiles of temperature, humidity, and wind, and surface pressure and sea surface temperature (SST)) are updated along the domain boundaries at 6-h intervals and the model time step is 90 s.

We ran RegCM3 simulations forced by the NCEP/NCAR Reanalysis output and SSTs from the National Oceanic and Atmospheric Administration (NOAA) weekly optimal interpolated sea surface temperature (OISST) data for the years 1982–2000. Weekly OISST data prior to 1982 are not available, so, to avoid mixing SST data sets, we limited the temporal coverage of the NCEP-forced RegCM3 simulations to this 19-year period. We use the NCEP-forced RegCM3 output to evaluate the global-regional model coupling, detailed in Sect. 3.1. We obtained global ECHAM5 output for 241 years (1860–2100) by combining the first runs (r1) of the twentieth century (years 1860–2000) and the IPCC AR4 Special Report on Emissions Scenarios A2 (years 2001–2100) experiments (Solomon et al. 2007). For ECHAM5, we focus on two 50-year periods: 1950–2000 (hereafter referred to as "present") and 2050–2100 (hereafter referred to as "future").

We will use the following nomenclature to identify the models and model data sets: NCEP refers to the NCEP/NCAR Reanalysis data; REG-NCEP refers to the RegCM3 simulations that were driven by NCEP for boundary conditions; ECHAM5 refers to the ECHAM5 global simulations; and REG-ECHAM5 refers to the RegCM3 simulations that were driven by ECHAM5 for boundary conditions.

2.2 Temporal and spatial pattern calculations

To enable the analysis of the PNA in the global and regional models, we explored two different approaches to compute the PNAI. We applied the modified pointwise method from the CPC (http://www.cpc.ncep.noaa.gov/products/precip/CWlink/pna/month_pna_index2.shtml), which is based on the pointwise method developed by Wallace and Gutzler (1981) but, instead of invariant point locations, incorporates regions of variability:

$$\begin{aligned}\mathrm{PNAI}_4 = \frac{1}{4}[&z^*(15-25^\circ\mathrm{N}, 180-140^\circ\mathrm{W}) \\ &-z^*(40-50^\circ\mathrm{N}, 180-140^\circ\mathrm{W}) \\ &+z^*(45-60^\circ\mathrm{N}, 125-105^\circ\mathrm{W}) \\ &-z^*(25-35^\circ\mathrm{N}, 90-70^\circ\mathrm{W})] \end{aligned} \quad (1)$$

where z^* is the 500-hPa standardized geopotential height anomaly. The four regions of high and low pressure in Eq. 1 are located near Hawai'i (subtropical high, "R0"), in the North Pacific (Aleutian low, "R1"), Western North America (continental high, "R2"), and the southeastern United States (southeastern low, "R3"). In RegCM3, R0 lies outside the domain, so we omitted R0 from Eq. 1

$$\begin{aligned}\mathrm{PNAI}_3 = \frac{1}{3}[&-z^*(40-50^\circ\mathrm{N}, 180-140^\circ\mathrm{W}) \\ &+z^*(45-60^\circ\mathrm{N}, 125-105^\circ\mathrm{W}) \\ &-z^*(25-35^\circ\mathrm{N}, 90-70^\circ\mathrm{W})] \end{aligned} \quad (2)$$

We found negligible differences between the PNAI_4 and PNAI_3 time series calculated from the global data: for the 1950–2000 period, the cross-correlation coefficient, r, for the two NCEP time series is 1.0, and the ECHAM5 time series are similarly correlated with $r = 0.99$ and $r = 0.98$ for 1950–2000 and 2050–2100, respectively. The close agreement between the PNAI_4 and PNAI_3 for NCEP and ECHAM5 is consistent with evidence indicating that the three regions, R1–R3 in Eq. 2, optimize the explanatory power of the PNA and the related wave energy propagation over North America (Leathers et al. 1991). We therefore focus on the regions R1–R3 and the PNAI_3 for our analysis.

We explore the spatial pattern of the PNA using linear regression maps. We regressed the standardized 500-hPa geopotential height anomalies (Z-scores) for the three-month period centered on the month of interest (that is, the standardized January 500-hPa geopotential anomalies are calculated using the DJF mean) against the DJF PNAI_3 time series for the respective model and period. Here we focus on the January pattern, as research and observations show that the PNA teleconnection is most prominent during the winter months (e.g. Wallace and Gutzler 1981; Leathers et al. 1991). The resulting maps display the amplitude of the January standardized 500-hPa anomalies associated with the DJF PNAI_3 time series.

The height of the 500–hPa pressure surface will increase as tropospheric temperatures increase from global warming.

To remove any temperature dependency of the 500–hPa heights that would bias the PNAI toward more positive values in the future (e.g. Cook et al. 2004; Lee et al. 2011), we standardized the anomalies used in the PNAI time series and the regression analysis based on their respective climatology period, that is, the index time series for the present (1950–2000) are standardized using the 1950–2000 climatology, whereas the time series for the future (2050–2100) are standardized using the 2050–2100 climatology.

3 Results and discussion

3.1 NCEP global and regional model coupling

Our regression map for the NCEP Reanalysis, which is essentially identical with that of the NCEP-CPC (http://www.cpc.ncep.noaa.gov/data/teledoc/pna_map.shtml), illustrates the spatial characteristics that typify the January PNA (Fig. 1a). Strong negative anomalies are centered on the trough associated with the Aleutian low at R1, strong positive anomalies are centered on the ridge associated with the continental high at R2, and slightly weaker negative anomalies are centered on the trough over the Gulf of Mexico and Southeast United States at R3. Our calculated PNAI time series for the NCEP data is similarly exactly the same as the time series from the CPC ($r = 1.0$, not shown; monthly CPC index values available at http://www.cpc.ncep.noaa.gov/products/precip/CWlink/pna/norm.mon.pna.wg.jan1950-current.ascii.table).

To establish the ability of the GCM-RCM coupled models to reproduce the PNA, we compare statistics of the 500-hPa heights used in the PNAI calculations, the PNAI time series, and the spatial patterns of composite anomalies for atmospheric and surface fields for the 1982–2000 NCEP Reanalysis and REG-NCEP simulations. Following Lin and Derome (1997), we computed the composite anomalies by subtracting the 1982–2000 mean from the mean of the positive PNA years (index values $> +0.5$; PNA+) and the mean of negative years (index values <-0.5; PNA−). The REG-NCEP statistics are in very good agreement with those of NCEP (Table 1). Roughly one-third of the area covered by R1 in Eq. 2 falls outside the domain of the RegCM3; constraining the NCEP averages to the area within the domain of the RegCM3 substantially improves the agreement at R1. For R2 and R3, the means and variability of the 500-hPa heights in NCEP and REG–NCEP agree well. The NCEP and RCM-NCEP time series (Fig. 2a) are highly correlated ($r = 0.99$). We attribute the small differences between the 1982–2000 NCEP and "NCEP on RCM GRID" statistics to slightly different simulations of 500-hPa geopotential heights associated with the atmospheric dynamics in the respective models and to how the boundary conditions from the GCM force the internal domain of the RegCM3.

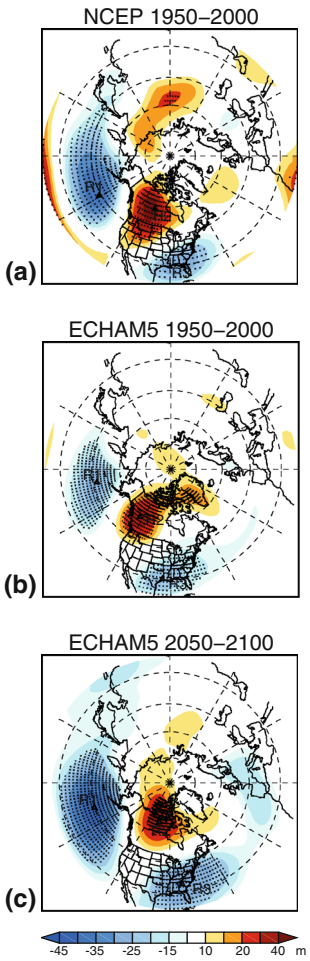

Fig. 1 The January PNA pattern shown as regression for **a** NCEP 1950–2000, **b** ECHAM5 1950–2000, and **c** ECHAM 2050–2100. The *centers* of R1, R2, and R3 are marked with *triangles*, and the *shaded areas* indicate significance at the 99.9 % level

The spatial patterns and the magnitudes of the composite anomalies for NCEP and REG-NCEP for both PNA+ (Fig. 3) and PNA− (Fig. 4) are in very good agreement, particularly the 500–hPa heights, temperature, and precipitation. The position and strength of the trough at R1, which lies along the boundary of the RCM, is strongly forced by the NCEP boundary conditions. In response, the RCM accurately develops the atmospheric structure of the upper level trough and surface low (not shown) of the Aleutian low. The 500-hPa wind anomalies clearly depict the differences in the flow around R1–R3 in the PNA+ and PNA− composites (Fig. 5). The pattern of cyclonic-anticyclonic-cyclonic anomalies for PNA+ contrasts with the opposite anticyclonic-cyclonic-anticyclonic pattern of the PNA− composite. The interplay of the flow around R1 and R2 in PNA+ results in advection of relatively warm air into the west and mid-continent from the south, which,

Table 1 Means and standard deviations (SD) of raw 500-hPa geopotential heights over each latitude-longitude region that were used to calculate the PNAI in both the global and regional simulations

Model	500-hPa geopotential heights: Mean ± SD (meters)		
	R1 (Aleutian low)	R2 (continental high)	R3 (Southeast US)
NCEP 1950-2000	5567 ± 166	5535 ± 152	5812 ± 79
NCEP 1982-2000	5564 ± 172	5543 ± 147	5818 ± 77
NCEP on RCM GRID	5586 ± 148	5549 ± 141	5822 ± 71
REG-NCEP	5591 ± 145	5543 ± 141	5817 ± 65
ECHAM5 1950–2000	5583 ± 170	5533 ± 135	5831 ± 77
ECHAM5 on RCM GRID	5588 ± 150	5535 ± 134	5832 ± 75
REG-ECHAM5	5588 ± 145	5503 ± 137	5808 ± 75
ECHAM5 2050-2100	5638 ± 187	5600 ± 136	5902 ± 87
ECHAM5 on RCM GRID	5647 ± 168	5601 ± 136	5903 ± 86
REG-ECHAM5	5642 ± 162	5569 ± 137	5869 ± 83

In the rows with three entries, the top entry is calculated on the more extensive GCM grid, the middle entry is calculated from GCM data that are regridded to the RegCM3 domain, and the third entry is calculated from the RCM simulations

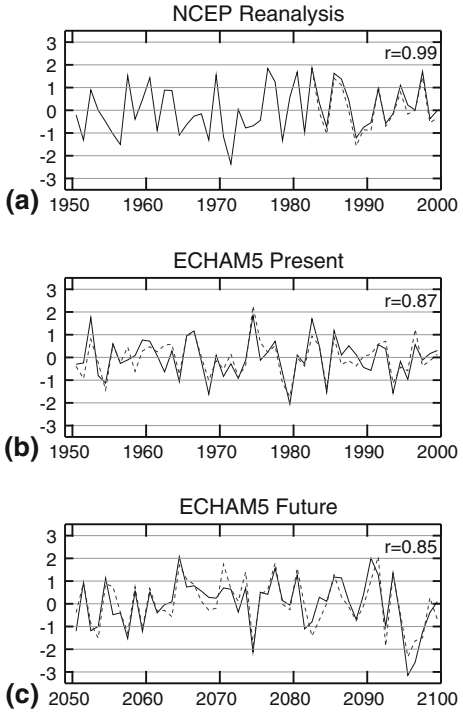

Fig. 2 PNAI time series for DJF for **a** NCEP Reanalysis years 1950–2000, **b** ECHAM5 years 1950–2000, and **c** ECHAM5 years 2050–2000. The *dotted lines* show the PNAI calculated from the REG-NCEP (1982–2000) and REG-ECHAM5 simulations using the 3-region method discussed in the text. The cross-correlation coefficients, *r*, indicate the agreement between the globally- and regionally-calculated time series

combined with compressional warming of sinking air under the high at R2, maintains the positive temperature anomalies. The southwesterly flow anomalies around R1 also create positive precipitation anomalies along the west coast of North America. An essentially opposite response is present for PNA−: northerly cold air advection over the Pacific Northwest and mid-continent maintains negative temperature anomalies and dry precipitation anomalies.

The anomalous temperature and precipitation patterns in PNA+ and PNA− years produce contrasting March SWE and April soil moisture patterns. Discrepancies between NCEP and REG–NCEP in the SWE and soil moisture fields in part reflect the differing resolutions of mountainous topography in western North America between the GCM and RCM, differences in the rate and location of precipitation (e.g. storms), and different surface physics in the models. The otherwise close agreement of NCEP and REG-NCEP indicates that the RegCM3 is capable of accurately downscaling the salient features of the positive and negative phases of the PNA.

3.2 500-hPa variability and change in ECHAM5 and REG-ECHAM5

The regression maps for the present-day NCEP and ECHAM5 simulations display similar spatial patterns over the NH (Fig. 1a, b). In ECHAM5, however, the magnitude of the anomalies at the centers of action are attenuated relative to NCEP by 10–15 m, there is a westward shift in R1, a southwestward shift in R2, and the area of positive anomalies over Northern Asia is not present, as in the NCEP data. By the end of the twenty first century, ECHAM5 simulates a relative strengthening and expansion of negative anomalies at R1 and R3, by 15 and 10 m, respectively (Fig. 1c). Additionally, the location of R1 shifts southward and is accompanied by a northeastward shift in the location of R2, while the future location of R3 remains similar to that of the present. The $\sim 20°$ increase in the north–south separation of R1 and R2 indicates stronger meridional flow, which is typically associated with positive PNA indices.

The magnitudes of the index values in the ECHAM5 time series compare well with the NCEP time series for both the present and future periods, with seasonal DJF values ranging between ± 3 (Fig. 2b, c). (The indices computed for the ECHAM5 simulations should capture the amplitude and frequency of the NCEP PNAI values; however, the value for any given month and year will differ relative to those of NCEP because the calendar in the ECHAM5 simulation is in model years). The cross-

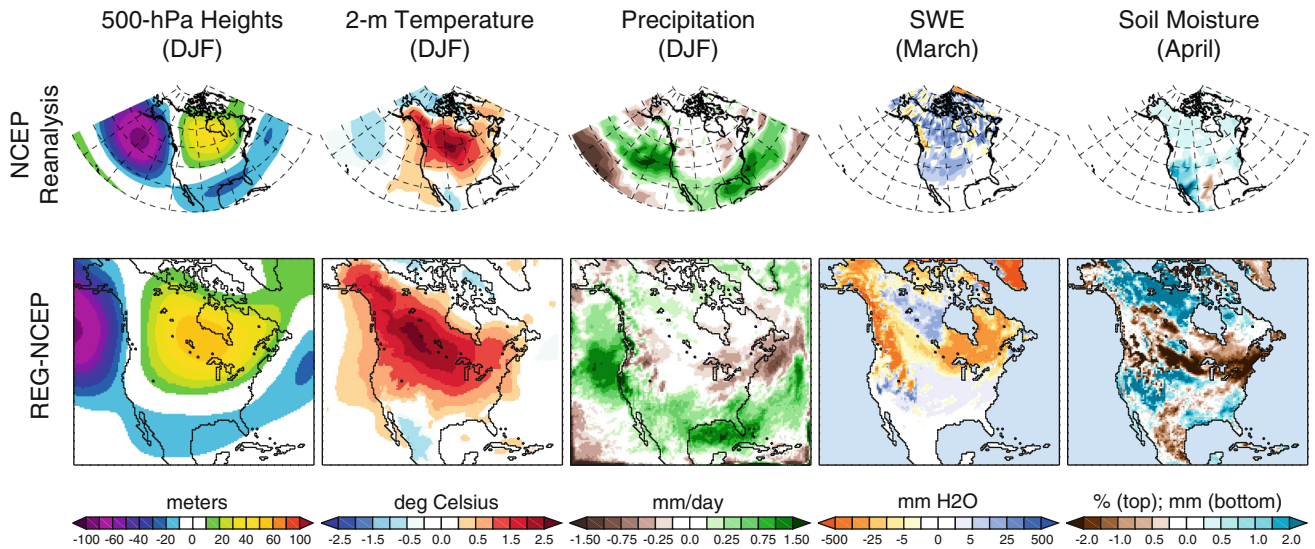

Fig. 3 Spatial patterns for PNA+ (indices > +0.5) composite anomalies for DJF 500-hPa geopotential heights, 2-m temperature, and precipitation, March snow water equivalent (SWE), and April soil moisture for NCEP Reanalysis and REG-NCEP years 1982–2000

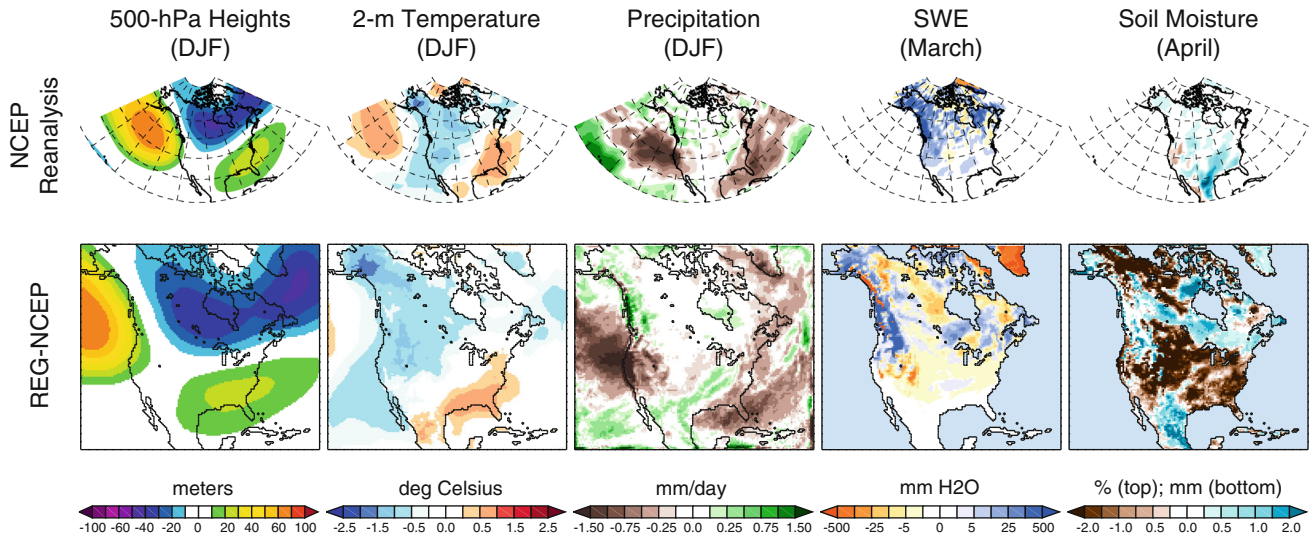

Fig. 4 As in Fig. 3, for PNA− (indices < −0.5) composite anomalies

correlation coefficients between the ECHAM5 and REG–ECHAM5 time series are 0.87 for 1950–2000 and 0.85 for 2050–2100. While these correlations are high, in addition to coverage of R1 in the RCM, the departures between the ECHAM5 and REG-ECHAM5 time series reflect weaker expression and displacement of the 500-hPa centers in ECHAM5, which translate into weaker internal forcing of REG-ECHAM5 relative to the REG-NCEP simulation.

The means and standard deviations of the 500-hPa heights in the 1950–2000 ECHAM5 and REG-ECHAM5 simulations are in good agreement both with each other and with those of the 1950–2000 NCEP data (Table 1); however, ECHAM5 produces weaker and fewer overall PNA+ events than are present in the NCEP data (Table 2, Fig. 2b). The mean and variability of the 500-hPa geopotential heights in each of the four regions increases by the end of the twenty first century as a result of greenhouse gas (GHG)-driven global warming (Table 1). In the ± 0.5 cutoff composites, there are 9 more PNA+ and 2 more PNA− events in the future, and the mean amplitude of PNA+ events decreases 8 %, whereas the mean amplitude of PNA− events increases by 25 % (Table 2; REG-ECHAM5 cutoff composite maps not shown). The expansion and strengthening of the trough-ridge-trough 500-hPa height anomalies around R1–R3 in the future ECHAM5 simulation (Fig. 6) explain the increase in future PNA+, consistent with recent trends toward more positive PNA events (e.g. Lee et al. 2011; Pederson et al. 2013) and the

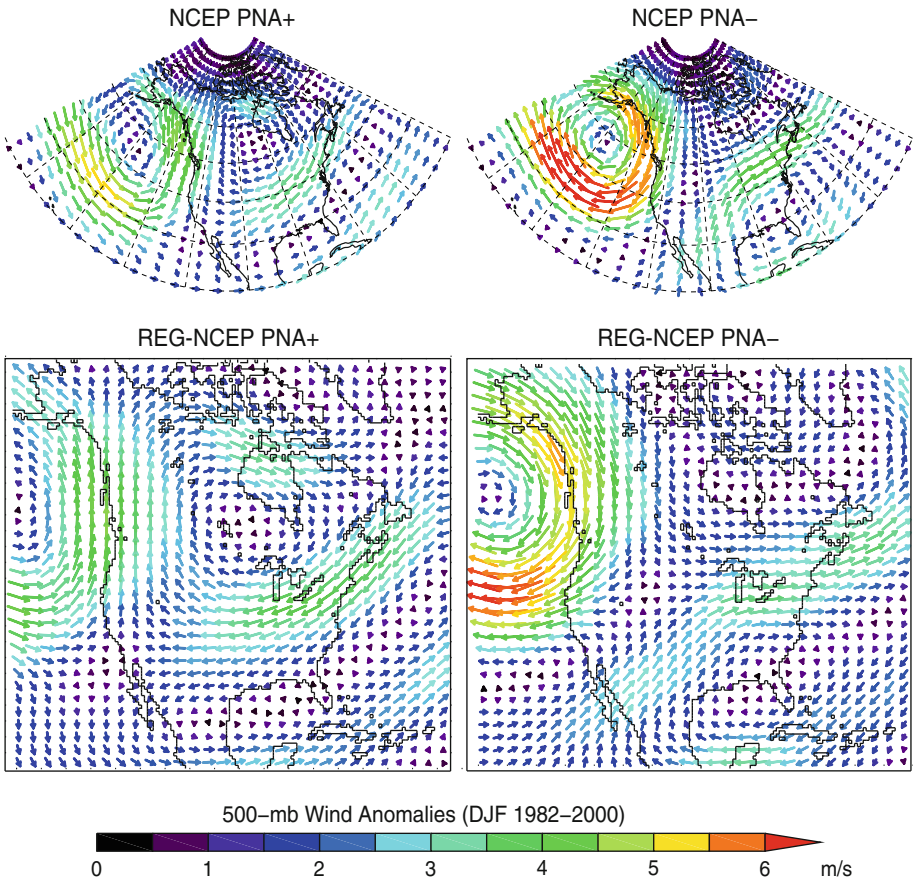

Fig. 5 Composite 500-hPa wind anomalies for NCEP and REG-NCEP for the years 1982–2000 for PNA+ (indices $> +0.5$) and PNA− (indices < -0.5)

behavior of the Aleutian low with the projected global warming (e.g. Bonsal et al. 2001; Salathé 2006).

3.3 Surface variability and change in REG-ECHAM5

To assess the PNA and associated surface fields in the REG-ECHAM5 simulations, we divided the ranked PNA time series into terciles and composited the top (bottom) 33 % of positive (negative) PNA years. Tercile-based composites provide fewer, higher magnitude events, and thus better separation of the range of PNA+ and PNA− than does the ± 0.5 cutoff, and they strike a balance between separating the events and having a sufficient number so that the composites are not dominated by one or two years (Table 2). Compared to 1950–2000, in the 2050–2100 simulation there are 2 more upper-tercile PNA+ events and a modest 2 % increase in the mean index amplitude, while in the lower tercile there is one fewer PNA− event and a 42 % increase in mean amplitude.

The spatial patterns of the 500-hPa anomalies for both the PNA+ and PNA− phases in the 1950–2000 REG-ECHAM5 simulations (Figs. 7a, 8a) are similar to those of the REG-NCEP simulation (Figs. 3a, 4a). Relative to REG-NCEP, both the PNA+ and PNA− 500-hPa anomaly maps for REG-ECHAM5 display westward shifts in the location of the centers of R1 and R2 that originate in the global ECHAM5 simulation (Fig. 1a, b). We cannot directly compare the REG-NCEP and REG-ECHAM5 simulations due to differences in the number of years in each composite (19 years in REG-NCEP versus 50 years in REG-ECHAM5). Nonetheless, the general spatial patterns of the surface climate variables are comparable, as an adequate number of positive and negative events are included in each time series to produce an accurate representation of the teleconnection pattern. Future changes in the DJF 500-hPa geopotential height anomalies for PNA+ and PNA− are substantial (Figs. 7a, 8a). Relative to the present, the area of significant influence of R1–R3 expands and the relative magnitude of the anomalies increase by $\sim$10 m, leading to associated anomalies in the 500-hPa winds (Fig. 9a). The expansion of R1 into the Pacific Northwest in the PNA+ and PNA− composites is in agreement with the eastward shift and deepening of the Aleutian low simulated by ECHAM5 in the future (Fig. 6).

The general spatial patterns of warm anomalies associated with the PNA+ and cool anomalies associated with PNA− (Figs. 7b, 8b) are comparable with those of the 1982–2000 REG-NCEP (Figs. 3b, 4b). Similar to geopotential heights, the regions with significant temperature anomalies in the PNA+ and PNA− composites expand in

Table 2 Mean values of the PNA+ and PNA− composites and the number of years included in the composite anomaly maps for the RegCM3 simulations

Model	±0.5 Cutoff composite Avg index value (# years in composite)		Tercile composite Avg index value (# years in composite)	
	PNA+	PNA−	PNA+	PNA−
NCEP (1950–2000)	1.29 (16)	−1.00 (18)	1.61 (8)	−1.26 (10)
NCEP (1982–2000)	1.35 (6)	−0.78 (5)	1.54 (4)	−0.92 (3)
ECHAM5 (1950–2000)	1.09 (11)	−1.07 (13)	1.27 (8)	−1.24 (9)
ECHAM5 (2050–2100)	1.00 (20)	−1.34 (15)	1.30 (10)	−1.77 (8)

The PNA+ cutoff composites include years with index values >0.5 and the PNA− cutoff composites include years with index values <−0.5. The tercile-based composites include years for the upper 33 % of the index values (PNA+) and the lower 33 % of the index values (PNA−). (REG-ECHAM5 cutoff composite maps and REG-NCEP tercile composite maps not shown)

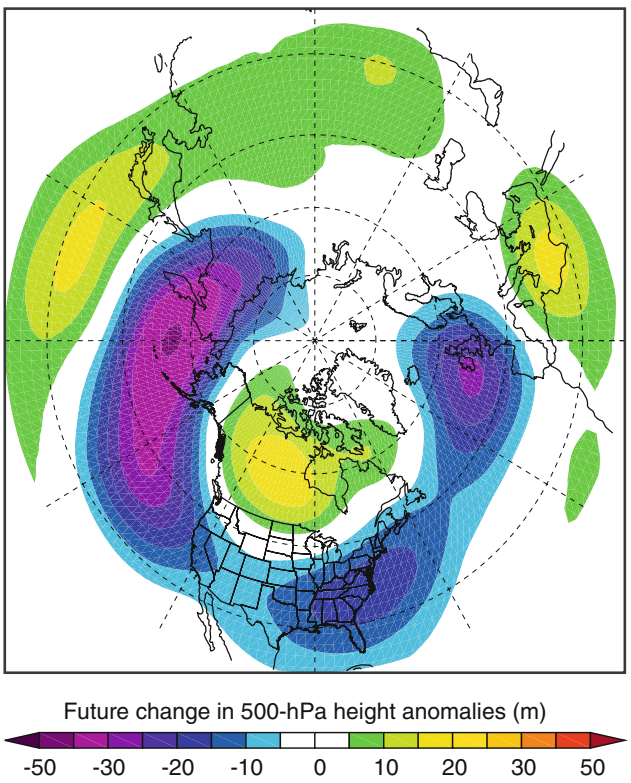

Fig. 6 Future anomalies (2050–2100 DJF minus annual mean) minus present anomalies (1950–2000 DJF minus annual mean) for ECHAM5 500-hPa geopotential heights

the future. In the PNA+, enhanced cyclonic flow over the West combined with enhanced anticyclonic flow around R2 leads to (relative) warm air advection, which spreads and shifts the distribution of warm anomalies. The increased influence of the future PNA+ creates larger warm anomalies throughout much of the Northwest, with magnitudes >2–2.5 °C in parts of northern Canada and Alaska. Future negative temperature anomalies of similar magnitudes associated with PNA− are also attributed to changes in circulation (Fig. 9b): enhanced anticyclonic flow over the West leads to cold air advection and reduced on-shore flow along the west coast, whereas significant warm anomalies >1 °C occur over the Southeast.

Future changes in precipitation anomalies are clearly related to the anomalies in circulation around R1–R3 (Figs. 7c, 8c, 9), but in both the PNA+ and PNA− composites the inherent variability in simulated precipitation reduces the extent of significance relative to temperature. Cyclonic wind anomalies along the west coast in the PNA+ composites that are associated with enhanced and significant wet anomalies ranging from 0.5 mm d^{-1} to >1 mm d^{-1} extend from the west coast, over the Basin and Range, and into the Central and Southern Rocky Mountains (Fig. 7c). In contrast, the anticyclonic anomalies in the PNA− wind flow along the west coast are associated with substantial drying on the order of −0.5 mm d^{-1} in these same regions, and the interplay of changes in the flow around R1–R3 combine to cause enhanced wet anomalies over Alaska, dry anomalies over Florida, and wet anomalies that extend from the southwest US to eastern Canada (Fig. 8c).

March SWE anomalies for the present are spatially similar and of opposite sign, contrasting the controls of circulation, temperature, and precipitation in the warm PNA+ and cold PNA− composites (Figs. 7d, 8d). The somewhat limited areas of significance in the SWE anomalies are an expression of the combined variability of precipitation and temperature in both phases, yet the spatially coherent patterns are meaningful indications of the regional controls of the PNA. In particular, the anomaly patterns of SWE over the mountainous regions of the West and Pacific Northwest illustrate the strong association of SWE with the PNA (Cayan 1996; Ge et al. 2009; Pederson et al. 2013) and the reinforcing or opposing controls of temperature and perception on snowpack are consistent with snowpack studies in the West (e.g. Hamlet et al. 2005; Mote et al. 2005; Kapnick and Hall 2010, 2012; Pederson et al. 2013).

The future SWE anomalies are broadly of the same sign as those of the present in the PNA+ and PNA− composites

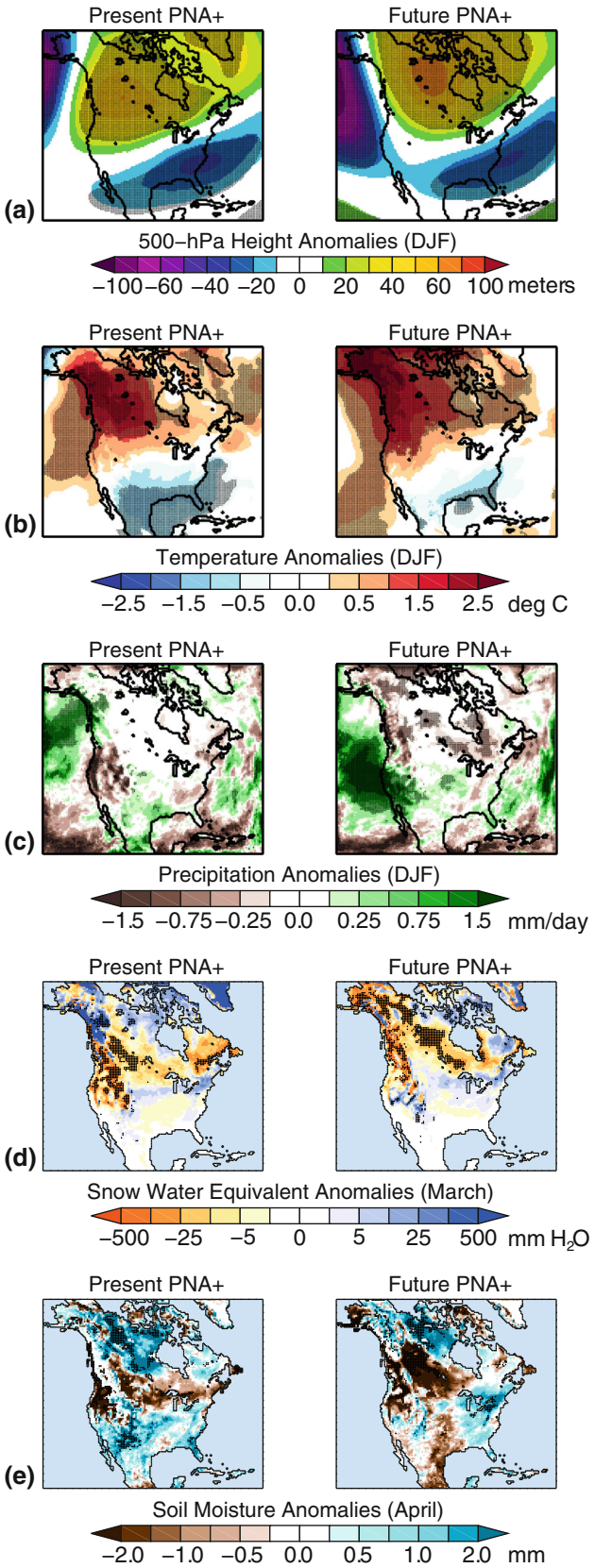

◀ **Fig. 7** Composite anomaly maps for the *upper tercile* of PNA indices (PNA+) for present (1950–2000, *left column*) and future (2050–2100, *right column*) ECHAM5 years. The variables shown are **a** 500-hPa geopotential heights, **b** 2-m air temperature, **c** precipitation, **d** March snow water equivalent (SWE), and **e** April soil moisture. *Shaded anomalies* are significant at the 90 % level

and, again, the patterns reflect changes in the distribution of temperature and precipitation (Figs. 7d, 8d). Warm and dry anomalies in the PNA+ composite extend from Alaska to the Pacific Northwest, where there is a corresponding reversal of sign in the SWE anomalies relative to the present, and positive precipitation anomalies over the Basin and Range and Southern Rocky Mountains support localized significant positive SWE anomalies. Negative precipitation anomalies in the PNA− composite result in negative SWE over the Basin and Range and Southern Rockies even though the future temperature anomalies are colder than those of the present. Over central and eastern Canada, future cold and wet anomalies lead to positive SWE anomalies where present SWE anomalies are negative. The future SWE anomalies in part reflect a general loss of snow as GHG warming alters the form of cold season precipitation (Fig. 10) and commences the melting of snowpack earlier in the spring. With the exception of Alaska, much of the high latitudes display little or no loss of SWE. Increased losses occur to the south and west, where the form of winter precipitation is strongly affected by the zero-degree Celsius isotherm.

In the regions where snow is a substantial component of the water budget, present April soil moisture anomalies generally correspond both with snowpack and precipitation anomalies (Figs. 7e, 8e). As is the case for SWE, the soil moisture anomalies display regional coherent patterns in both the PNA+ and PNA− composites, but variability in snowpack and precipitation limit the extent of significance. In the present PNA+ composite, there is a general alternating north-to-south pattern of wet/dry/wet anomalies and localized negative anomalies over the Pacific Northwest and some areas of the Northern Rocky Mountains. This pattern is essentially reversed in the PNA− composite. The DJF precipitation and March SWE anomalies control soil moisture in the Pacific Northwest, the Basin and Range, the Rocky Mountains, and the higher latitudes of Canada in the present and future composites; however, in both cases, the soil moisture anomalies over the Southwest and particularly the eastern US cannot be explained by winter snowpack or precipitation. Coleman and Rogers (2003) found that anomalously wet (dry) winters associated with strong PNA− (PNA+) events do not typically have a strong influence on the Ohio River Valley spring soil moisture,

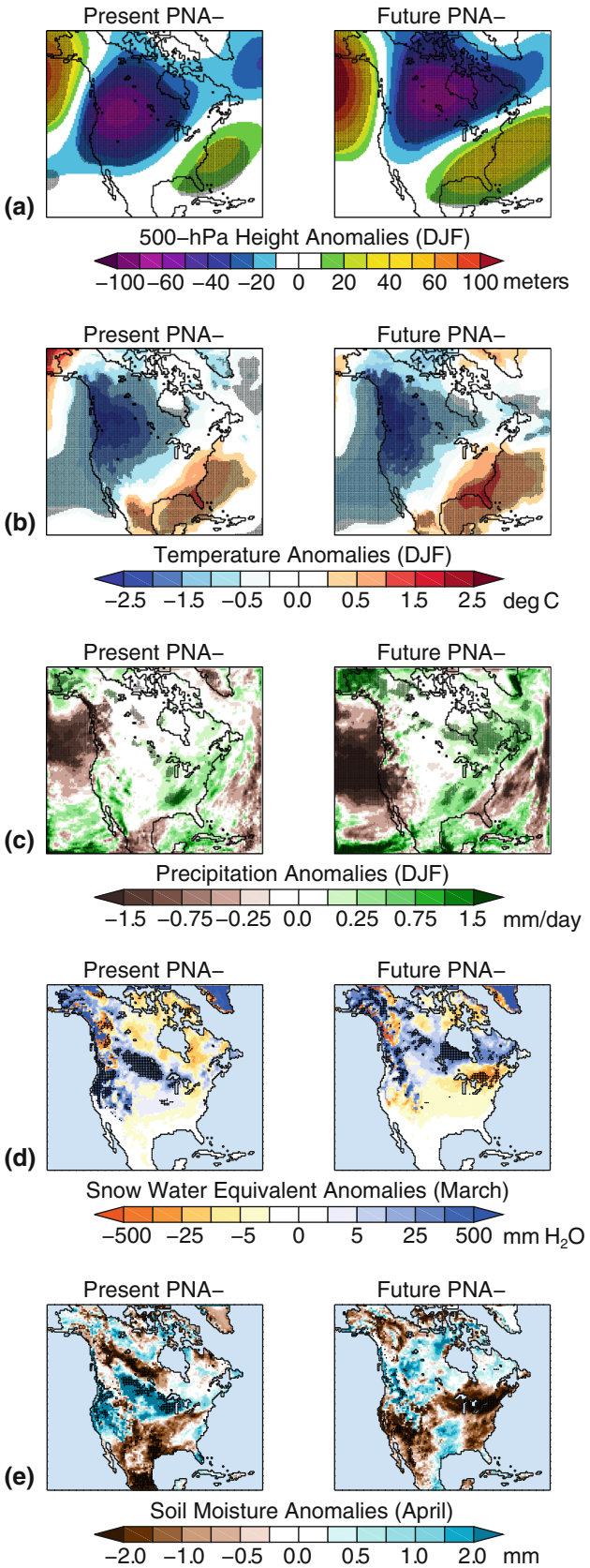

Fig. 8 As in Fig. 7, for the *bottom tercile* of PNA indices (PNA−)

which instead is driven by spring PNA precipitation anomalies. Our RegCM3 simulations are consistent with Coleman and Rogers (2003), as the present and future April soil moisture anomalies over the mid-continent and the East clearly reflect the April precipitation anomalies rather than the DJF precipitation anomalies, particularly in the PNA− composite (Fig. 11). Soil moisture over the Pacific Northwest is also enhanced by April precipitation anomalies during the cold PNA− phase which, depending on elevation, falls either as liquid or spring snow.

4 Summary

The PNA is expressed as a prominent large-scale atmospheric circulation pattern in both the NCEP/NCAR Reanalysis and the ECHAM5 GCM. The spatial patterns of the present 1950–2000 and future 2050–2100 ECHAM5 PNA are similar to those of NCEP; although, the strength of the teleconnection in the present ECHAM5 simulation is weaker than NCEP. The future 2050–2100 ECHAM5 PNA strengthens substantially and consequently has a stronger influence over future North American climate. The future spatial orientation of the pressure centers shifts slightly in response to a significant expansion of the Aleutian low at the end of the twenty first century, leading to more significant changes in surface climate variables. As a result, the relative influence of the PNA teleconnection on future climate is spatially enhanced, particularly for PNA+ events, reinforcing projections of more frequent positive PNA indices in the future.

The key characteristics of the PNA from the global models are resolved with little loss of information when downscaled by the RegCM3 RCM. Comparisons between the 1982–2000 500-hPa heights and surface climate anomalies between NCEP and REG-NCEP indicate strong representation of the spatial patterns associated with positive and negative PNA phases by RegCM3. A high correlation exists between the PNAI calculated with the NCEP Reanalysis data and the REG-NCEP output, which reveals the ability of the RCM to reproduce the spatial characteristics of the PNA and also to reproduce the amount of variability in the associated 500-hPa heights. Similar agreement exists between the ECHAM5 and REG-ECHAM PNAI for the present and future periods, although slightly lower correlation coefficients reflect weaker expression and displacement of the 500-hPa centers relative to NCEP.

Surface climate anomalies are consistent with the spatial pattern of 500-hPa heights associated with the PNA for temperature and precipitation. The significant areas of influence of the PNA generally expand in the future, primarily due to the expansion of the Aleutian low, which is

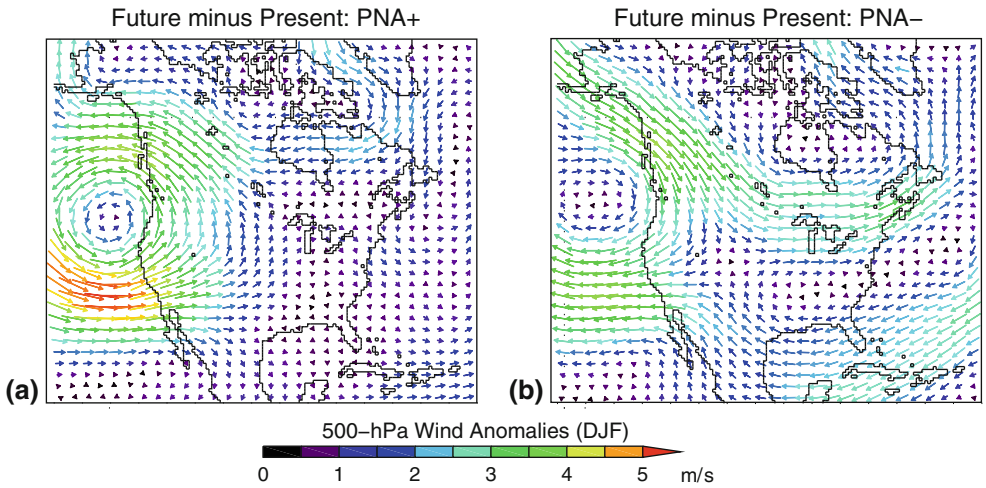

Fig. 9 Future (2050–2100) minus present (1950–2000) DJF 500-hPa wind vector anomalies for **a** *upper tercile* (PNA+) and **b** *lower tercile* (PNA−) composites

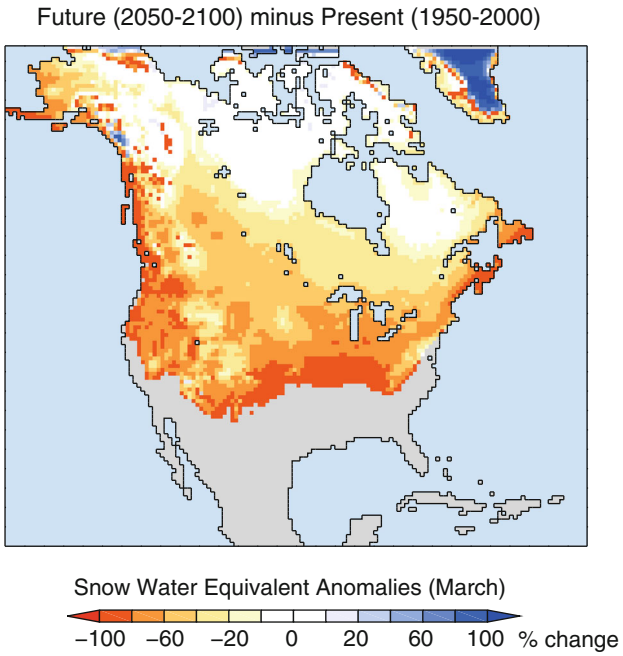

Fig. 10 Future (2050–2100) minus present (1950–2000) change in mean March snow water equivalent in the REG-ECHAM5 simulations. *Gray* areas have <1 mm snow water equivalent in the present day simulation

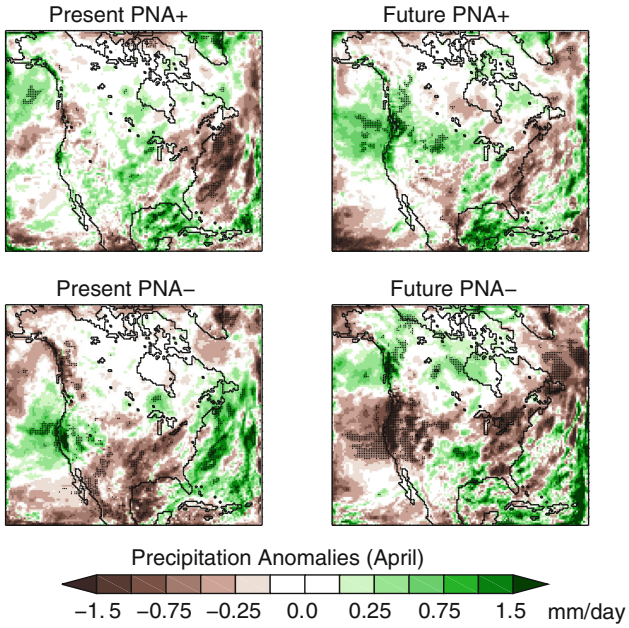

Fig. 11 Composite April precipitation anomaly maps for the *upper* (PNA+) and *lower* (PNA−) tercile of PNA indices for present (1950–2000, *left column*) and future (2050–2100, *right column*) REG-ECHAM5 years. *Shaded anomalies* are significant at the 90 % level

reflected in the 500-hPa winds. Increased circulation off the west coast increases warm (cold) air advection and brings significant increases (decreases) in precipitation to western North America during strong PNA+ (PNA−) events. The combined influences of temperature and precipitation drive changes in March SWE, particularly in the Pacific Northwest. April soil moisture anomalies generally follow trends in March SWE anomalies; however, in regions without persistent snowpack, April soil moisture anomalies more closely reflect April precipitation anomalies. From these analyses, we can conclude that the future PNA remains an important influence on surface climate in North America.

While our study is limited to the NCEP/NCAR Reanalysis and one GCM, the success of the global-regional model coupling is encouraging for future global and regional modeling endeavors. The ability of a regional model to downscale global atmospheric circulation patterns such as the PNA is promising for the assessment of regional climate changes, especially as global climate models and the techniques of dynamical downscaling continue to improve.

Acknowledgments We thank the journal reviewers for their comments and suggestions. We acknowledge the NCEP/NCAR Reanalysis Project for providing access to the reanalysis data and we thank the Max Planck Institute for Meteorologie for providing the 20C and A2 ECHAM5 data. The Oregon State University College of Earth, Ocean, and Atmospheric Sciences Computing Center provided the infrastructure and support for our regional model simulations and the Climate and Land Use Program of the United States Geological Survey provided funding for this research.

References

Abatzoglou JT (2010) Influence of the PNA on declining mountain snowpack in the Western United States. Int J Clim 31(8): 1–8

Barnston AG, Livezey RE (1987) Classification, seasonality and persistence of low-frequency atmospheric circulation patterns. Mon Weather Rev 115:1083–1126

Bonsal BR, Shabbar A, Higuchi K (2001) Impacts of low frequency variability modes on Canadian winter temperature. Intl J Clim 21:95–108

Cayan DR (1996) Interannual climate variability and snowpack in the Western United States. J Clim 9:928–948

Coleman JSM, Rogers JC (2003) Ohio River Valley winter moisture conditions associated with the Pacific-North American teleconnection pattern. J Clim 16:969–981

Cook ER, Woodhouse CA, Eakin CM, Meko DM, Stahle DW (2004) Long-term aridity changes in the Western United States. Science 5:1015–1018

Dickinson R, Henderson-Sellers A, Kennedy P (1993) Biosphere-atmosphere transfer scheme (BATS) version 1e as coupled to the NCAR Community Climate Model, Technical Report, Natl Cent for Atmos Res

Fauria MM, Johnson EA (2008) Climate and wildfires in the North American boreal forest. Philos Trans of R Soc Biol Sci 363:2315–2327

Feldstein S (2000) The timescale, power spectra, and climate noise properties of teleconnection patterns. J Clim 13:4430–4440

Ge Y, Gong G, Frei A (2009) Physical mechanisms linking the winter Pacific-North American teleconnection pattern to spring North American snow depth. J Clim 22:5135–5148

Grell G (1993) Prognostic evaluation of assumptions used by cumulus parameterizations. Mon Weather Rev 121:764–787

Hamlet AF, Mote PW, Clark MP, Lettenmaier DP (2005) Effects of temperature and precipitation variability on snowpack trends in the western United States. J Clim 18:4545–4561

Jungclaus JH, Botzet M, Haak H, Keenlyside N, Luo J–J, Latif M, Marotzke J, Mikolajewicz U, Roeckner E (2005) Ocean circulation and tropical variability in the AOGCM ECHAM5/ MPI-OM. J Clim 19:3952–3972

Kalnay E, Kanamitsu M, Kistler R et al (1996) The NCEP/NCAR 40-year reanalysis project. Bull Am Met Soc 77:437–471

Kapnick S, Hall A (2010) Observed climate-snowpack relationshipsin California and their implications for the future. J Clim 23(13):3446–3456

Kapnick S, Hall A (2012) Causes of recent changes in western North American snowpack. Clim Dyn 38:1885–1899

Kawamura R, Sugi M, Sato N (1995) Interdecadal and interannual variability in the Northern extratropical circulation simulated with the JMA global model. Part I: wintertime leading mode. J Clim 8:3006–3019

L'Heureux ML, Kumar A, Bell GD, Halpert MS, Higgins RW (2008) Role of the Pacific-North American (PNA) pattern in the 2007 Arctic sea ice decline. Geophys Res Lett 35:1–5

Lau N-C (1981) A diagnostic study of recurrent meteorological anomalies appearing in a 15-year simulation with a GFDL general circulation model. Mon Weather Rev 109:2287–2311

Leathers DJ, Palecki MA (1992) The Pacific/North American teleconnection pattern and United States climate. Part II: temporal characteristics and index specification. J Clim 5:707–716

Leathers DJ, Yarnal B, Palecki MA (1991) The Pacific/North American teleconnection pattern and United States climate. Part I: regional temperature and precipitation associations. J Clim 4:517–528

Lee S, Gong G, Johnson N, Feldstein SB, Pollard D (2011) On the possible link between tropical convection and the Northern Hemisphere arctic surface air temperature change between 1958 and 2001. J Clim 24:4350–4367

Lin H, Derome J (1997) On the modification of the high- and low-frequency eddies associated with the PNA anomaly: an observational study. Tellus 49A:87–99

Marsland SJ, Haak H, Jungclaus JH, Latif M, Röske F (2003) The Max Planck Institute global ocean/sea-ice model with orthogonal curvilinear coordinates. Ocean Model 5:91–127

McCabe GJ, Wolock DM (2010) Long-term variability in Northern Hemisphere snow cover and associations with warmer winters. Clim Change 99:141–153

Mote PW, Hamlet AF, Clark MP, Lettenmaier DP (2005) Declining mountain snowpack in western North America. Bull Am Met Soc 86:39–49

Müller WA, Roeckner E (2006) ENSO impact on midlatitude circulation patterns in future climate change projections. Geophys Res Lett 33:1–4

Notaro M, Wang W-C, Gong W (2006) Model and observational analysis of the Northeast U.S. regional climate and its relationship to the PNA and NAO patterns during early winter. Mon Weather Rev 134:3479–3505

Pal J, Small E, Eltahir E (2000) Simulation of regional-scale water and energy budgets: representation of subgrid cloud and precipitation processes within RegCM. J Geophys Res Atmos 105:29579–29594

Pal JS et al (2007) Regional climate modeling for the developing world: the ICTP RegCM3 and RegCNET. Bull Am Met Soc 88:1395–1409

Pederson GT, Betancourt JL, McCabe GJ (2013) Regional patterns and proximal causes of the recent snowpack decline in the rocky mountains. U.S. Geophys Res Lett 40:1–6

Roeckner E, Bäuml G, Bonaventura L, Brokopf R, Esch M, Giorgetta M, Hagemann S, KirchneR I, Kornblueh L, Manzini E, Rhodin A, Schlese U, Schulzweida U, Tompkins A (2003) The atmospheric general circulation model ECHAM5. Part I: model description Rep. 349. Max Planck Institute for Meteorology, Hamburg, pp 1–127

Salathé EP (2006) Influences of a shift in North Pacific storm tracks on western North America precipitation under global warming. Geo Res Lett 33:1–4

Solomon S, Qin D, Manning M et al. (2007) IPCC Climate Change 2007: The Physical Science Basis. Contribution of Working Group I to the Fourth Assessment Report of the Intergovernmental Panel on Climate Change. Cambridge University Press, Cambridge, United Kingdom and New York, NY, USA

Stoner AMK, Hayhoe K, Wuebbles DJ (2009) Assessing general circulation model simulations of atmospheric teleconnection patterns. J Clim 22:4348–4372

Wallace JM, Gutzler DS (1981) Teleconnections in the geopotential height field during the Northern Hemisphere winter. Mon Weather Rev 109:784–812

Yu B, Zwiers FW (2007) The impact of combined ENSO and PDO on the PNA climate: a 1, 000-year climate modeling study. Clim Dyn 29:837–851